Materials Advances

ROYAL SOCIETY OF CHEMISTRY

PAPER

View Article Online
View Journal | View Issue

Check for updates

Cite this: *Mater. Adv.*, 2024, 5, 3838

Modification of chitosan-coated magnetic material with glycidyltrimethylammonium chloride and its application as heterogeneous base catalyst for levulinic acid esterification†

Feri Mukhayani,[a] Yuichi Kamiya,*[b] Ryoichi Otomo,[b] Eko Sri Kunarti[a] and Nuryono Nuryono*[a]

Received 22nd February 2024,
Accepted 16th March 2024

DOI: 10.1039/d4ma00181h

rsc.li/materials-advances

To promote more widespread use of biodiesel, it is essential to add additives to improve its fuel properties, and one such additive is ethyl levulinate (EL). EL is often produced by acid-catalyzed esterification of levulinic acid (LA) with ethanol, but acid catalysis has a critical problem of low catalytic activity. This problem can be solved by using a base catalyst for this reaction. In the present study, we developed a novel composite material that was composed of natural magnetic material (MM), which was obtained from iron sand, with chitosan (Chi) and glycidyltrimethylammonium chloride (GTMAC), and applied it as a base catalyst for esterification of LA to EL. In the first step, the surface of MM was modified with chitosan in 1% acetic acid, and then it was further modified with GTMAC at room temperature. The obtained composite (MM/Chi/GTMAC) was comprehensively characterized by various physical and chemical methods to verify that it had a core (MM)–shell (Chi/GTMAC) structure as expected. In addition, TPD measurements demonstrated that MM/Chi/GTMAC had base sites owing to chloride ions in GTMAC. MM/Chi/GTMAC exhibited high catalytic performance for esterification of LA to EL and 77% of EL yield, and 89% of LA conversion were achieved at 80 °C for 6 h, while MM and MM/Chi showed only little catalytic activity for EL formation. Additionally, the catalyst was reusable, while the performance was gradually decreased with each repeated use for the reaction.

1. Introduction

Essential points that should be considered for developing and using biofuel are the amount of produced energy, reduced greenhouse gas emissions, and, of course, its production cost.[1] Biodiesel is one of the most popular biofuels that can replace fossil fuels in the transport and fuel sector. Compared to conventional diesel oil produced from petroleum, the sulfur content in biodiesel is low. Thus, its combustion produces less SO_2 emission, avoiding acid rain and photochemical smog, which is currently caused by the combustion of fossil fuels.[2] Thus, expansion of biodiesel utilization can reduce the negative environmental impact caused by fuel combustion. Although biodiesel has many advantages over conventional diesel oil, it has the same problem of generating soot during combustion as conventional diesel oil. To avoid soot generation, additives that have high oxygen content must be added to biodiesel. One biodiesel additive with sufficient oxygen content is ethyl levulinate (EL),[3] whose oxygen content is 33 wt%. In addition to reducing the soot generation, advantages of EL as a biodiesel additive include improvement in lubricity, flash point stability, reduction of sulfur content,[4,5] and decrease of viscosity of biodiesel.[6]

The development of practical methods and processes for the production of EL is still keenly desired. Levulinic acid (LA) is one of the platform chemicals produced from biomass[7] and is utilized as a raw material for the production of EL. EL is usually synthesized by esterification of LA with ethanol (EtOH) in the presence of a catalyst,[8] and homogeneous and heterogeneous acid catalysts promote this reaction. Commonly used homogeneous catalysts are mineral acids such as sulfonic acid, sulfuric acid, and hydrochloric acid, but they have disadvantages of not being reusable, difficulty in separation from the solution,[9] and hazardous and high cost.[2] Therefore, many researchers tried to develop and apply heterogeneous acid catalysts, namely solid acid catalysts, including sulfonated lignin-based carbon catalysts,[10] sulfonic acid-functionalized

---

[a] *Department of Chemistry, Universitas Gadjah Mada, 55281, Yogyakarta, Indonesia. E-mail: nuryono_mipa@ugm.ac.id*
[b] *Faculty of Environmental Earth Science, Hokkaido University, 060-0810, Sapporo, Japan. E-mail: kamiya@ees.hokudai.ac.jp*

† Electronic supplementary information (ESI) available. See DOI: **https://doi.org/10.1039/d4ma00181h**

silica,[11,12] and Amberlyst-15[13] for the reaction. Indeed, solid acid catalysts promoted the reaction with high selectivity to EL, even under mild reaction conditions.[14] Nevertheless, the acid catalysts still have a critical problem of low catalytic activity, regardless of homogeneous or heterogeneous form.[15]

Therefore, researchers have investigated base catalysts for the reaction to overcome the problems with acid catalysts, while the research is only a little compared to the acid ones. Heterogeneous base catalysts such as CaO,[16] MgO–CaO,[17] and SrO[18] were applied for transesterification reactions. Therefore, we were interested in developing heterogeneous base catalysts that are active for the esterification of LA with EtOH.

Previous research demonstrated that chloride ion (Cl^-)-intercalated MgAl-layered double hydroxide acted as a solid catalyst for the hydrolysis of carbonyl sulfide.[19] A report showed that adding chloride ions to Li/SnO_2 improved the catalytic performance for the conversion reaction of chloromethane to ethylene.[20] Those previous studies suggest that chloride ion gives a base site in the materials. Based on this speculation, we focused on glycidyltrimethylammonium chloride (GTMAC) as an active component for a base function to support materials. GTMAC is a compound with an epoxide group at one end and a quaternary ammonium at the other. Unique points of this compound are that chloride ions at the quaternary ammonium cation are known to act as a Lewis base site, and an epoxide group is usable to fix this compound tightly to support materials through a covalent bond. As a support material for GTMAC, magnetite/silica,[21] chitosan,[22] and polyvinyl alcohol (PVA) membranes[23] have been investigated. Among them, chitosan is one of the most attractive materials because of its high biocompatibility, biodegradability, and environmentally friendliness.[24,25] In addition to a base function, easy separation is also essential in a solid base catalyst for practical applications. Environmentally benign natural magnetic materials help to provide magnetic properties to solid catalysts, so the catalysts are separated simply by applying an external magnetic field.

In the present study, we synthesized a magnetically separable heterogeneous base catalyst in which natural magnetic material was modified sequentially with chitosan and GTMAC, and the synthesized catalysts were thoroughly characterized by physical and chemical methods. Furthermore, the catalysts were applied for the esterification of LA with EtOH to EL, and a kinetic study was done for the reaction over the catalyst.

2. Experimental section

2.1 Chemicals

Natural magnetic material (MM) was isolated from iron sand collected from Meliwis Beach, Kebumen, Central Java, Indonesia, containing iron oxide as a main component (70 wt%) and was treated as previously reported[26] as follows. The iron sand (25 g, 200 mesh) was heated in 50 mL of 1 M HCl solution at 60 °C for 5 h, and then 1 M of NaOH solution was added to the mixture until pH 10. The precipitate was collected by filtration and washed with distilled water until the filtrate became neutral. After that, it was dried at 90 °C for 10 h, and MM was obtained.

The following chemicals were used for the synthesis of the materials, which included chitosan powder (75–85% deacetylated, Merck), GTMAC (Sigma Aldrich), acetic acid (Merck), and sodium hydroxide (Merck). The chemicals used for the catalytic reaction (LA, EtOH, EL, and *o*-xylene) were purchased from Wako Pure Chemical Co. All the reagents were used as received.

2.2 Synthesis of magnetically separable heterogeneous base catalyst (MM/Chi/GTMAC)

Chitosan powder (0.5 g) was dissolved in 50 mL of 1 mass% acetic acid solution, and the mixture was stirred for 15 min until chitosan power was completely dissolved.[27] To the solution, 3 mL of 1 M HCl solution containing 1.5 g of MM was poured, and the resulting suspension was treated with ultrasonication for 10 min. Then, the mixture was stirred at 60 °C for 4 h. After that, 1 M of aqueous NaOH solution was added until the pH of the mixture was 10, and a precipitate of chitosan-modified MM, which is named MM/Chi, was formed. The precipitate was collected by filtration and washed with distilled water until the filtrate became pH 7.

The modification of MM/Chi with GTMAC was performed as follows: 1.5 mL of GTMAC was added to 1.75 g of MM/Chi, and the mixture was stirred at room temperature for 1 h. Afterward, the resulting solid was separated by an external magnet, washed with distilled water two times (50 mL × 2), and dried in an oven at 90 °C for 10 h. The obtained material is named MM/Chi/GTMAC.

2.3 Characterization

The synthesized materials were thoroughly characterized using FTIR-ATR, XPS, XRD, TGA, FE-SEM, and TEM. FTIR spectra of the materials were taken on a Fourier transform infrared-attenuated total reflection (FTIR-ATR) spectrometer (NICOLET, Is10 Thermi Gisher Scientific) in the 400–4000 cm^{-1} range. The resolution and number of scans were 0.5 cm^{-1} and 16, respectively. The electronic states of elements in the materials were investigated using XPS spectroscopy. Before measurement, all samples were coated with Pt–Pd to impart conductivity. The XPS spectra were obtained with a JEOL JPS_9200 spectrometer using an aluminum anode, and the scanning range was 0–1000 eV. XRD patterns of the materials were taken on an X-ray diffractometer (Bruker, D2 PHASER 2nd Generation) with Cu Kα radiation operating at 30 kV and 10 mA in the range of 2θ = 5–90° at a scanning rate of 0.02° min^{-1}. Thermogravimetric analysis (TGA) of the materials was performed using a Pyris 1 TGA thermal analyzer (PerkinElmer). The temperature was increased from room temperature to 500 °C at 10 °C min^{-1} in air flow (50 mL min^{-1}). The morphologies and EDX mapping of the materials were observed using a JEOL JSM-6510LA SEM microscope operating at 5 kV and 30 mA. To afford measurements, the material was coated with Au. The core–shell structure of the material was identified using transmission electron microscopy (TEM, EM Philips EM 208S). The TEM specimens were prepared by dispersing the sample powder in ethanol and placing a drop of the dispersion liquid onto a carbon-coated copper grid.

The materials were also characterized using a surface area and pore size analyzer, zeta-sizer, VSM, CO_2-TPD, and ion-chromatograph. Surface area, pore volume, and pore size distribution were estimated from N_2 adsorption–desorption isotherm taken at −196 °C on a Micrometrics ASAP analyzer. Before measurement, the samples were pretreated at 200 °C in a vacuum. The Brunauer–Emmett–Teller theory was applied to determine the specific surface area of the materials. For zeta-sizer measurement, 5 mg of material was dispersed in 10 mL of citric acid solution (1%), and the suspension was treated under sonication for 15 min. The analysis was performed by transferring 1.5 mL of the sample solution into a disposable folding capillary cuvette. Zeta potential and particle size were measured simultaneously using Malvern zeta-sizer Pro-Red MAL1266214 with a 293 nm laser. The refractive index and the detection angle were set at 1.493–1.509 and 173°, respectively. The measurement was performed three times at room temperature, and the average was taken. The magnetic properties of the materials were evaluated using a superconducting quantum interference device (SQUID) MPMS-5 (Quantum Design) magnetometer at room temperature. The VSM hysteresis curve was scanned with the range of magnetic field between −20 000 Oe (−2 T) and 20000 Oe (2 T) at a scanning speed of 0.1 T min^{-1}. CO_2-TPD was performed to analyze the basicity of the materials, and a BelCAT instrument (Bel Japan) was used for the measurement. About 0.1 g of the sample was placed in a quartz reactor and pretreated in a He flow (25 mL min^{-1}) at 200 °C for 48 min. The sample was then cooled to 35 °C in CO_2 flow (25 mL min^{-1}), followed by saturation of the sample with CO_2 at 40 °C for 35 min. Desorption of CO_2 was carried out by heating the sample up to 400 °C at a heating rate of 10 °C min^{-1}. The concentration of chloride ions in the materials was determined using an ion chromatograph (TOSOH, IC-8100) equipped with an electrical conductivity detector. The solid sample (0.05 g) was added to 2 mmol L^{-1} of NaBr solution to release Cl^- from the sample, and then the filtrate was analyzed by the ion chromatograph to determine the concentration of Cl^- in the solution.

2.4 Evaluation of catalytic performance

Esterification of LA with EtOH in the presence of MM/Chi/GTMAC was performed in a test tube heated in an aluminum block heater. Typically, 0.567 g (5 mmol) of LA and 3.945 g (86 mmol) of EtOH were charged in a test tube with the catalyst. The reaction was performed with different catalyst masses (15 and 30 mg) and reaction time (1, 2, 3, 6, 8, 9, 10, 20, and 24 h) to investigate their effects on the reaction. After the reaction, the catalyst was separated with an external magnet, and the obtained reaction solution was analyzed by a gas-chromatograph (Shimadzu, GC-2014) equipped with a flame ionization detector (FID) and a capillary column (Restek, SH-Rtx-Wax). Quantifications of the unreacted LA and produced EL were carried out with an internal standard method using *o*-xylene as an internal standard. The conversion of LA and yield of EL were calculated with eqn (1) and (2), respectively.

$$\text{Conversion of LA (\%)} = \frac{\text{mass of LA}_{\text{initial}} - \text{mass of LA}_{\text{final}}}{\text{mass of LA}_{\text{initial}}} \times 100 \tag{1}$$

$$\text{Yield of EL(\%)} = \frac{\text{amount of EL}}{\text{amount of LA}_{\text{initial}}} \times 100 \tag{2}$$

2.5 Recycling test

After a reaction, the catalyst was separated with an external magnet and washed three times with 5 mL of ethanol. After drying in an oven at 60 °C for 10 h, the catalyst was used for the second. The recycling test was performed up to 4 times, namely, first-time use and three times reuse.

2.6 Kinetic model for the esterification of LA

The esterification of LA with EtOH is a reversible reaction, as shown in eqn (3), and the whole reaction rate equation is expressed in eqn (4),

$$\text{LA + EtOH} \rightleftarrows \text{EL + H}_2\text{O} \tag{3}$$

$$-r_{\text{LA}} = -\frac{\text{d}C_{\text{LA}}}{\text{d}t} = k_1 C_{\text{LA}}{}^{\alpha} C_{\text{EtOH}}{}^{\beta} - k_2 C_{\text{EL}}{}^{\gamma} C_{\text{water}}{}^{\delta} \tag{4}$$

where C_{LA}, C_{EtOH}, C_{EL}, and C_{water} are the concentrations of LA, EtOH, EL, and water, respectively, at a particular time, α, β, γ, and δ are reaction orders with respect to each component, and k_1 and k_2 are rate constants for the forward and reverse reactions, respectively. Since ethanol was excess, in this study, the reaction was considered that (1) the concentration of ethanol was constant and (2) the equilibrium was largely shifted, and thus the reverse reaction could be ignored in the low conversion of LA. Therefore, eqn (4) can be simplified to eqn (5).

$$-\frac{\text{d}C_{\text{LA}}}{\text{d}t} = k_1' C_{\text{LA}}{}^{\alpha} \tag{5}$$

Eqn (5) can be integrated according to the value of α as eqn (6)–(8), having α = 0, 1, and 2, respectively,

$$xC_{\text{LA}(0)} = k_{1.0}' t \tag{6}$$

$$-\ln(1 - x) = k_{1.1}' t \tag{7}$$

$$\frac{1}{1 - x} = C_{\text{LA}(0)} k_{1.2}' t \tag{8}$$

where x is the conversion of LA, $C_{\text{LA}(0)}$ is initial LA concentration, and $k_{1.0}'$, $k_{1.1}'$, and $k_{1.2}'$ are pseudo-zero, pseudo-first, and pseudo-second-order rate constants, respectively. These three equations have been used in previous studies for kinetic analysis,[10,11,28,29] and the reaction order was determined by fitting the experimental data using those reaction equations.

3. Results and discussion

3.1 Characterization of the synthesized materials

XRD analysis. Measurement of XRD patterns for the synthesized materials was performed to obtain information on their crystal structures. The XRD patterns of MM, chitosan, MM/Chi, and MM/Chi/GTMAC are presented in Fig. 1(a). Most diffraction lines for MM were assigned to magnetite (Fe_3O_4), which were indexed as (220), (311), (400), (422), (511) and (440) planes,[30,31] while there were some weak diffraction lines that could not be assigned to magnetite. MM/Chi and MM/Chi/GTMAC gave basically the same XRD patterns as MM, indicating that the modifications of MM with chitosan and GTMAC did not change the structure of MM in the core. The diffraction line intensities for MM/Chi and MM/Chi/GTMAC were slightly weaker than those for MM. This decrease was mainly because the magnetite content was low in MM/Chi and MM/Chi/GTMAC due to chitosan and GTMAC. It should be noted that there was no diffraction line due to crystalline chitosan, which must appear at around $2\theta = 10$ and 20°, for MM/Chi, indicating that crystalline chitosan turned to amorphous in an acetic acid solution, which might help it to disperse highly on MM.

FTIR analysis. Next, the formation of and changes in the functional groups by the modification of MM with chitosan and GTMAC were examined by FTIR. The IR spectra of MM, chitosan, MM/Chi, and MM/Chi/GTMAC are shown in Fig. 1(b). On the spectrum of MM, a strong absorption band due to skeletal vibration of Fe–O was observed at 580 cm^{-1}. As previously reported,[32,33] chitosan gives several characteristic absorption bands that correspond to stretching of N–H and O–H at around 3400 cm^{-1}, CO-stretching (amide I) at 1655 cm^{-1}, and bending of –NH (amide-II) at 1590 cm^{-1}. In addition to them, symmetrical stretching of C–H, bending of $-CH_2-$, symmetrical deformation of $-CH_3$, and asymmetric stretching of C–O–C were observed at 2924, 1420, 1375, and 1077 cm^{-1}, respectively. On the spectrum of MM/Chi, the absorption band characteristics to chitosan were observed, while the band due to CO-stretching (amide I) of chitosan was shifted to 1575 cm^{-1}, and the bending of $-CH_2-$ appeared at 1422 cm^{-1}. Those band shifts indicated that chitosan interacted with MM, presumably through the hydroxyl group on MM.

Pour *et al.* reported that GTMAC showed IR bands of the epoxide group, stretching of NR_4^+ complexes, and symmetrical bending of $-CH_3$ on the quaternary ammonium substituent appeared at 880–980, 600–1000 and 1475 cm^{-1}, respectively.[34] These absorption bands were observed for MM/Chi/GTMAC, but the band of the epoxide group disappeared, indicating the opening of the epoxide ring. Therefore, GTMAC was fixed by the reaction of the epoxide, presumably with $-NH_2$ in chitosan, to make a covalent N–C bond.

XPS analysis. Fig. 2 shows high-resolution XPS N1s spectra of chitosan, MM/Chi, and MM/Chi/GTMAC with curve fitting results. The chitosan used in this study has two nitrogen-containing functional groups, primary amine and amide, but it only had a peak at 397.4 eV.[35] On the other hand, the

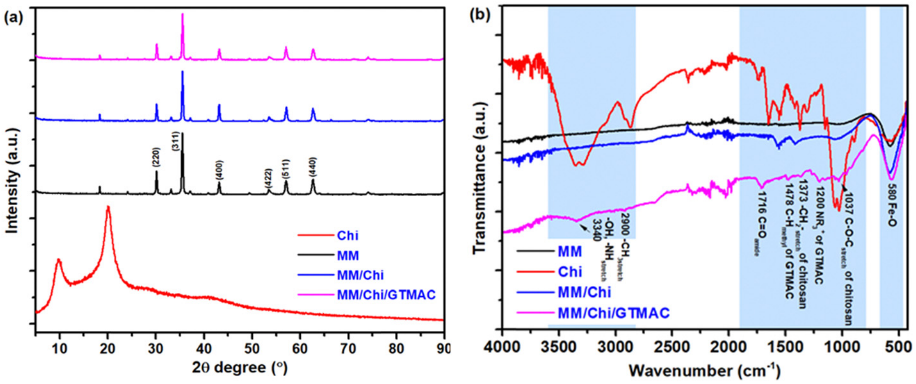

Fig. 1 (a) Powder XRD patterns and (b) IR spectra of MM, chitosan, MM/Chi, and MM/Chi/GTMAC.

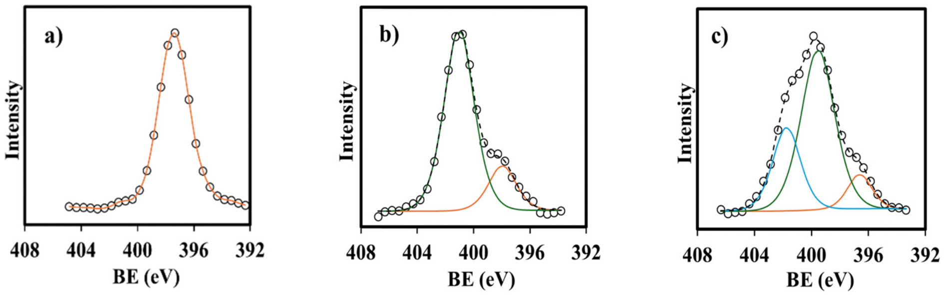

Fig. 2 High resolution XPS N1s spectra of (a) chitosan, (b) MM/Chi, and (c) MM/Chi/GTMAC.

Table 1 Zeta potential and particle size of MM, Chitosan, GTMAC, MM/Chi, and MM/Chi/GTMAC

Material	Zeta potential (mV)	Particle size (nm)
MM	−11.7	1575
MM/Chi	34.1	651
MM/Chi/GTMAC	36.2	1428
Chitosan	39.4	743
GTMAC	5.5	768

spectrum of MM/Chi showed two peaks at 398.0 and 401.0 eV, which were assignable to intact nitrogen-containing functional groups of chitosan and those that interacted with the surface of MM, respectively. According to the peak area ratio, about 82% of the nitrogen-containing functional groups of chitosan interacted with the MM surface, presumably through hydrogen bonding. It should be noted that MM/Chi/GTMAC had three peaks at 396.6, 399.5, and 401.7 eV, whose peak areas corresponded to 10%, 63%, and 27%, respectively. Considering the electronic state of nitrogen, the nitrogen of quaternary ammonium cation ($-N(CH_3)_3^+$) in GTMAC is more positively charged than those of amine and amide of chitosan, even if they interacted with the surface of MM. Therefore, it is reasonable that the peak at 401.7 eV was attributed to $-N(CH_3)_3^+$, while the peaks at 396.6 and 399.5 eV were assigned to the intact and interacted nitrogen-containing functional groups of chitosan, respectively.[36,37] The slight change in the binding energies for the nitrogen-containing functional groups of chitosan by the modification with GTMAC was probably due to the presence of GTMAC. Based on these results and discussion, it can be concluded that GTMAC was successfully introduced in MM/Chi/GTMAC, which is then tested as a solid base-catalyst for esterification of LA to LE.

Zeta potential and particle size. Zeta potentials and average particle size of the synthesized materials are listed in Table 1. As a reference, data on chitosan and GTMAC are also included in the table.

The particle size of MM was 1575 nm. It is known that magnetite particles like MM tend to aggregate very easily owing to strong hydrogen bonding,[37] causing attraction between the particles.[38] The modification of MM with chitosan decreased the particle size, which was 651 nm. Considering pK_a, almost all amino groups in chitosan are present as amino cations ($-NH_3^+$) in solution at pH 4.[39] Since the modification of MM with chitosan was performed in 1 M hydrochloric acid, the amino group of chitosan in MM/Chi must exist as $-NH_3^+$, causing electrostatic repulsion between the particles. In addition, covering the surface of MM further weakened the interaction due to hydrogen bonding that acted by the surface hydroxyl groups of MM. At higher pH levels, the number of $-NH_3^+$ and the net of the interchain repulsive electrostatic forces are reduced. Hydrogen bonding and hydrophobic interactions between chains would be favored.[40,41] This can promote the formation of a more compact structure, so the particle size of the material becomes smaller. By those effects, the aggregation of the MM particles was eliminated with the chitosan modification, decreasing the particle size of the material (MM/Chi). However, the particle size was significantly increased by the modification of MM/Chi with GTMAC. This is because GTMAC covered the surface of MM/Chi, thereby weakening the effect brought about by chitosan.

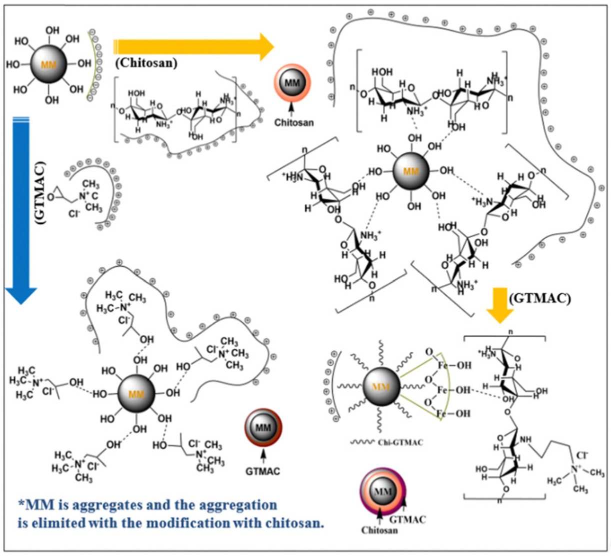

*MM is aggregates and the aggregation is elimited with the modification with chitosan.

Fig. 3 Images of structures and surface charges of MM, chitosan, GTMAC, MM/Chi, MM/GTMAC, and MM/Chi/GTMAC.

A schematic image of the structures of the materials in each preparation step speculated based on zeta potential is proposed in Fig. 3. As Table 1 shows, MM had a zeta potential of −11.7 mV, indicating that a lot of hydroxyl groups were present on the surface. On the other hand, the zeta potential of chitosan was 39.4 mV, meaning that the surface of chitosan was positively charged.

Chitosan is a positively charged polymer with polar functional groups such as $-NH_2$ and $-OH$.[38] In an acidic solution like 1% citric acid, those polar functional groups of chitosan undergo protonation to give a positive charge on the surface. Chitosan is a polycation, and its charge density changes depending on the degree of acetylation and pH of the solution. Large amounts of protonated $-NH_2$ groups, namely $-NH_3^+$, on the chitosan structure account for its solubility in acid-aqueous media since its pK_a is approximately 6.5. Chitosan becomes soluble when around 50% of the amino groups are protonated.[42]

GTMAC also had positive zeta potential, being 5.5 mV, and it was due to the presence of quaternary ammonium cations ($-N(CH_3)_3^+$). The modification of MM with chitosan and GTMAC changed the zeta potential of the materials. MM/Chi had a zeta potential of 34.1 mV, meaning the surface was positively charged in an acidic solution. The drastic change in the zeta potential with the modification of MM with chitosan indicated that the surface of MM was successfully covered with chitosan. It should be noted that MM/Chi/GTMAC had zeta potential that was more positive than those of MM/Chi and MM/GTMAC. This indicates that the positive charges of

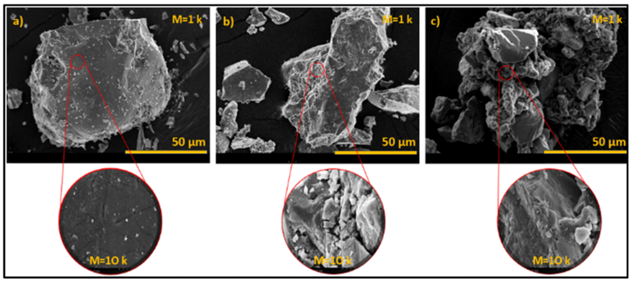

Fig. 4 SEM images of (a) MM, (b) MM/Chi and (c) MM/Chi/GTMAC.

chitosan and GTMAC contributed together to produce a more significant positive charge on the surface since a large amount of positively charged organic compounds was present on the surface of MM/Chi/GTMAC.

Morphology. The morphologies of the materials, including MM, MM/Chi, and MM/Chi/GTMAC were observed by SEM (Fig. 4). As Fig. 4(a) demonstrates, MM had a smooth surface. Magnetic material often grew in an octahedral shape.[43,44] Comparing the SEM image of MM/Chi (Fig. 4(b)) with that of MM (Fig. 4(a)), it was obvious that chitosan formed some aggregates on the surface of MM/Chi. The material became denser after the modification with GTMAC (Fig. 4(c)). These SEM images demonstrate that the MM surface was successfully covered with chitosan and GTMAC, demonstrating that MM/Chi/GTMAC had a core–shell structure, where MM and chitosan/GTMAC formed the core and shell, respectively.

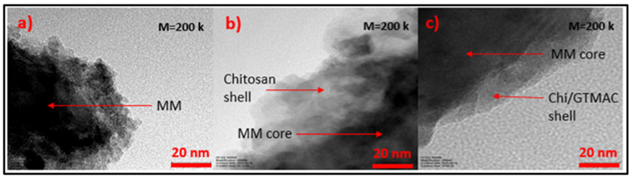

Fig. 5 TEM images of (a) MM, (b) MM/Chi and (c) MM/Chi/GTMAC.

Fig. 5 displays the detailed morphologies of MM, MM/Chi, and MM/Chi/GTMAC observed by TEM. In Fig. 5(b), it was clearly observed that the MM core was covered with the chitosan shell. The thickness of the shell became thinner after the modification with GTMAC (Fig. 5(c)). This is because GTMAC was strongly bound to chitosan on the MM surface, and the structure became very dense.

The EDX spectra and elemental EDX mapping of MM, MM/Chi, and MM/Chi/GTMAC are given in Fig. 6. It is obvious that MM contained Fe and O, while C and N were present in MM/Chi in addition to Fe and O. Moreover, the EDX spectrum for MM/Chi/GTMAC demonstrated the presence of more amounts of C and N in MM/Chi/GTMAC. It is noted that Cl was detected only for MM/Chi/GTMAC, demonstrating the successful modification with GTMAC. These sequentially decrease content in the Fe composition (MM > MM/Chi > MM/Chi/GTMAC) strongly supported the formation of ideal core (MM)–shell (Chi/GTMAC) structure.

Thermal stability. Fig. 7(a) shows TG profiles taken in air for MM, MM/Chi, and MM/Chi/GTMAC. MM showed almost no weight loss over the temperature. On the other hand, MM/Chi lost weight by 9.2% in the temperature of 200–275 °C, which was attributable to the thermal decomposition of chitosan in MM/Chi. From the weight loss at 500 °C, the amount of

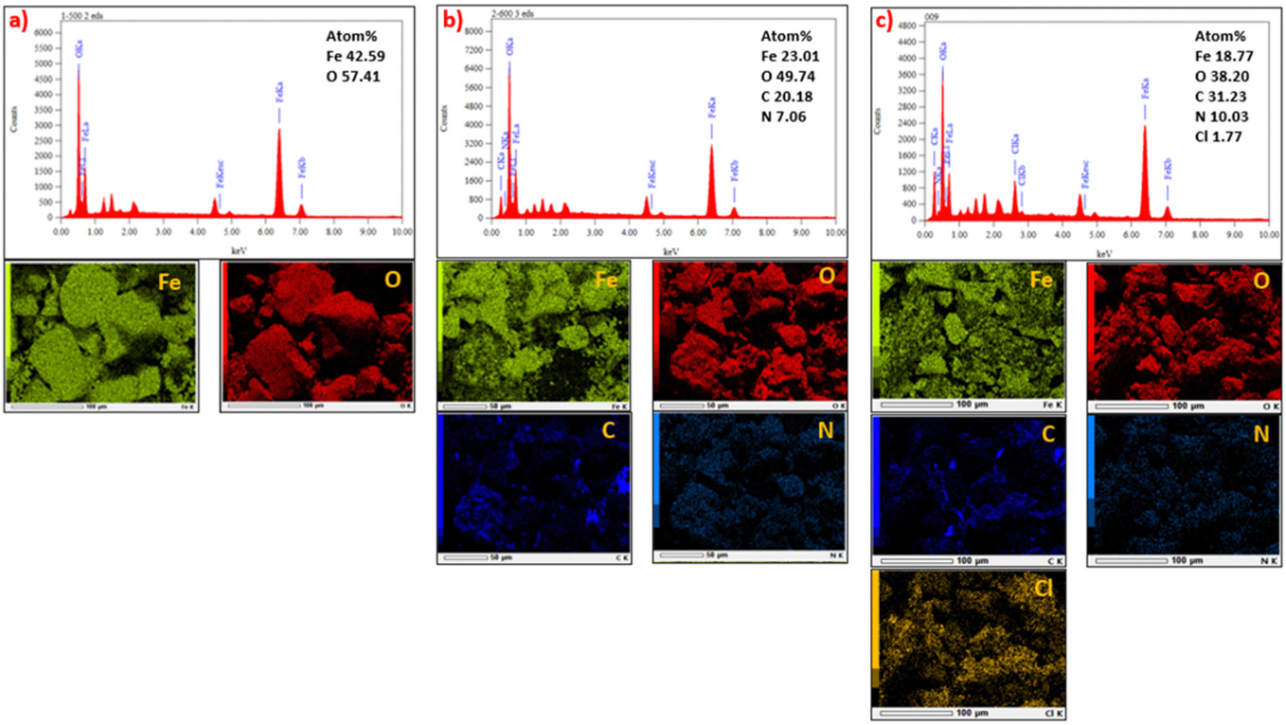

Fig. 6 EDX spectra and elemental mappings for (a) MM, (b) MM/Chi and (c) MM/Chi/GTMAC.

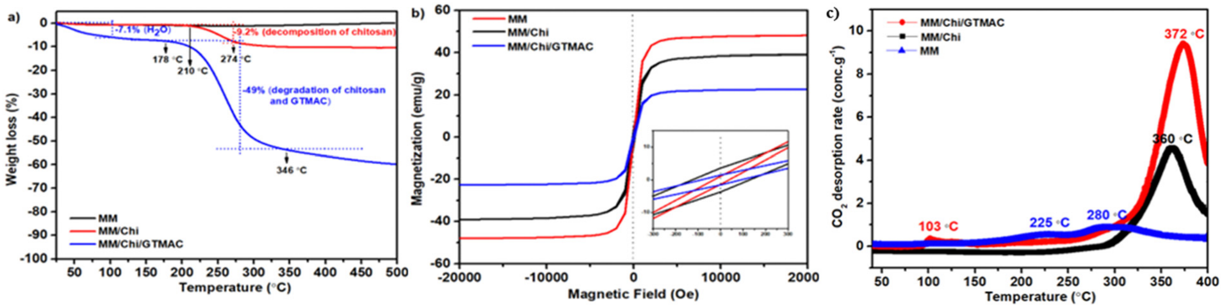

Fig. 7 (a) TG profiles, (b) VSM hysteresis curves, and (c) CO_2-TPD of MM, MM/Chi, and MM/Chi/GTMAC.

chitosan present in MM/Chi was estimated to be 9.2 wt%. For MM/Chi/GTMAC, the weight loss proceeded in two steps. The first weight loss proceeded from room temperature to about 100 °C due to the desorption of physisorbed water, suggesting that the surface of MM/Chi/GTMAC was hydrophilic. The second weight loss occurred at 180–350 °C due to the thermal decomposition of chitosan and GTMAC. In other words, MM/Chi/GTMAC was thermally stable up to 180 °C. Since the difference in the weight loss between 178 and 346 °C was 49%, and the amount of chitosan was 9.2 wt%, that of GTMAC in MM/Chi/GTMAC was estimated to be 39.8 wt%.

Magnetic property. The magnetic properties of MM, MM/Chi, and MM/Chi/GTMAC were investigated using a SQUID magnetometer at room temperature (Fig. 7(b)). The superparamagnetic properties of MM, MM/Chi, and MM/Chi/GTMAC were determined based on the magnetic hysteresis curve, which was determined from the relationship between magnetization and an external magnetic field. For materials to be applied as a catalyst, the magnetism of the catalyst is an essential property for easy separation from the reaction solution.[45] Pristine MM had saturation magnetization value of 44.09 emu g^{-1}, which was almost the same as that of a common magnetite (around 50 emu g^{-1}).[45,46] The saturation magnetization values of MM/Chi and MM/Chi/GTMAC were 38.10 and 22.01 emu g^{-1}, respectively. Hence, the modification of MM with chitosan and GTMAC decreased the saturation magnetization value as expected. However, MM/Chi/GTMAC still had enough magnetism for magnetic separation.

Basicity. Number of base site of the catalyst must largely influence the catalytic performance for the esterification of LA. Thus, the number of base site of MM/Chi/GTMAC was investigated by CO_2-TPD, in which CO_2 is a commonly used probe molecule to assess the basicity of solid materials. Fig. 7(c) shows CO_2-TPD profiles of MM, MM/Chi, and MM/Chi/GTMAC. MM gave two small peaks at 225 and 280 °C, indicating that MM had only a small number of base sites. In contrast, MM/Chi and MM/Chi/GTMAC exhibited a large desorption peak at 360 and 372 °C, respectively. Since no peak appeared for MM/Chi/GTMAC without CO_2 adsorption (Fig. S1 in ESI†), those large peaks were attributed to the base sites on MM/Chi/GTMAC. However, the desorption temperature of CO_2 was higher than its heat resistance temperature. From the peak areas, the numbers of the base sites on MM/Chi and MM/Chi/GTMAC were estimated to be 0.28 and 0.58 mmol g^{-1}, respectively. It is reported that GTMAC had Lewis basicity, which is brought by chloride ions. Therefore, the large number of the base sites in MM/Chi/GTMAC was due to the presence of Cl^- in this material in addition to amino groups of chitosan. To confirm this, the amount of Cl^- in MM/Chi/GTMAC was quantified using an ion chromatograph (see Experimental section) and was 0.46 mmol g^{-1}, a little less than the number of base sites estimated by CO_2-TPD.

Surface area and porosity. The surface area and porosity of the synthesized materials were characterized with BET (surface area, S_{BET}, and pore volume, V_{BET}) and BJH (average pore radius, R_p) theories, respectively. As shown in Fig. 8, all the materials exhibited a type IV isotherm, indicating the presence of mesopores. The surface area, pore volume, and average pore radius are listed in Table 2. The modification of MM with chitosan and GTMAC decreased both surface area and pore

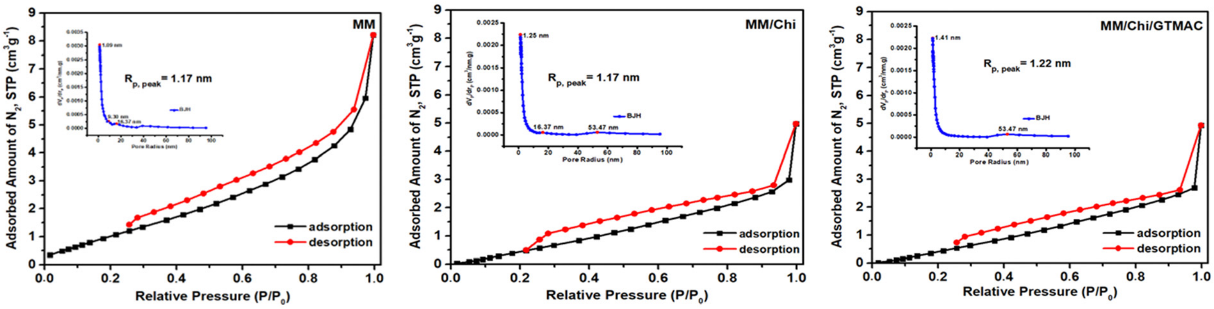

Fig. 8 Nitrogen adsorption–desorption isotherms for MM, MM/Chi, and MM/Chi/GTMAC.

Table 2 Surface area and pore characteristics of MM, MM/Chi, and MM/Chi/GTMAC

Material	S_{BET} (m^2 g^{-1})	V_{BET} (mm^3 g^{-1})	R_p (nm)
MM	5.20	12.0	1.17
MM/Chi	4.02	6.4	1.17
MM/Chi/GTMAC	3.95	6.2	1.22

volume, suggesting that chitosan and/or GTMAC covered the surface of MM in MM/Chi and MM/Chi/GTMAC.

Chemical structure of MM/Chi/GTMAC. Based on the characterization data described so far, again we proposed the chemical structure of MM/Chi/GTMAC as Fig. 3. MM was activated with acid in advance, and the surface of the pristine MM had many hydroxyl groups. Since chitosan is a compound with hydroxyl and amino groups, can interact with MM through hydrogen bonding, forming $-NH_3^+\cdots HO^-$. GTMAC interacted with chitosan through covalent bond formation by epoxide-ring opening, which made GTMAC tightly attach to the surface of MM/Chi, giving MM/Chi/GTMAC.

3.2 Catalytic performance of MM/Chi/GTMAC for esterification of levulinic acid with ethanol

Plausible reaction mechanism for esterification of levulinic acid and ethanol over MM/Chi/GTMAC. Before showing the catalytic reaction data, a plausible reaction mechanism for the reaction on MM/Chi/GTMAC is explained in Fig. 9. As was demonstrated, chloride ion (Cl^-) on MM/Chi/GTMAC exhibited basicity, which must be Lewis base. The process in the esterification of LA on Lewis base sites includes (1) adsorption of LA and EtOH on the catalyst; (2) abstraction of proton of hydroxyl group in EtOH by a Lewis base site to form ethoxide anion; (3) nucleophilic attack of the ethoxide anion to the carbonyl group to form a good leaving group and donation of an electron pair on the oxygen atom in the hydroxyl group to the carbon to regenerate carbonyl group, and elimination of H_2O; (4) desorption of formed EL from the catalyst.

Catalytic performance of MM/Chi/GTMAC. The catalytic performance of MM/Chi/GTMAC was evaluated with esterification of LA with EtOH at 80 °C with a molar ratio of EtOH to LA of 17 (EtOH/LA = 17). Fig. 10 shows the time courses of the conversion of LA and yield of EL for the reaction with different MM/Chi/GTMAC masses (2.5 and 5.0 wt%). As shown in Fig. 10, LA was converted to EL, and the conversion and yield were increased with reaction time regardless of the catalyst mass. It is noted that an increase of the catalyst mass from 2.5 to 5 wt% increased EL yield accordingly. However, using a large amount of the catalyst (5 wt%) caused only minor enhancements in the conversion and yield, probably because the reaction reached near equilibrium even with 2.5 wt% catalyst mass. The reaction with 5 wt% mass of MM/Chi/GTMAC exhibited 77% yield of EL and 89% conversion of LA at 6 h. Prolonged reaction time did not decrease the yield of EL, indicating that no successive reaction of EL occurred. Under the same reaction conditions, MM and MM/Chi showed only a very low yield of EL, 2.5 and 2.0%, respectively, while the conversions were 23 and 30%, respectively. These results clearly demonstrated that the Lewis base site, owing to Cl^- in GTMAC on MM/Chi/GTMAC, but not amine groups in chitosan, were the effective active sites for the esterification of LA to EL.

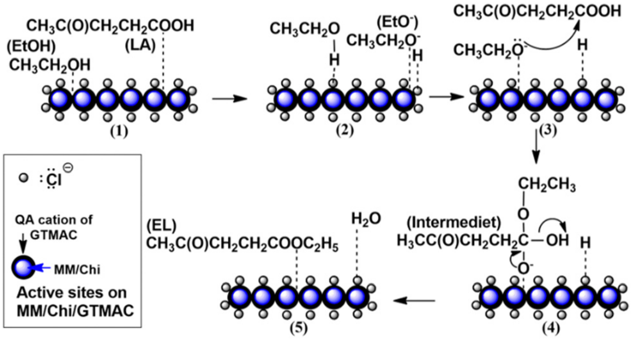

Fig. 9 A plausible reaction mechanism for esterification of LA with EtOH over MM/Chi/GTMAC.

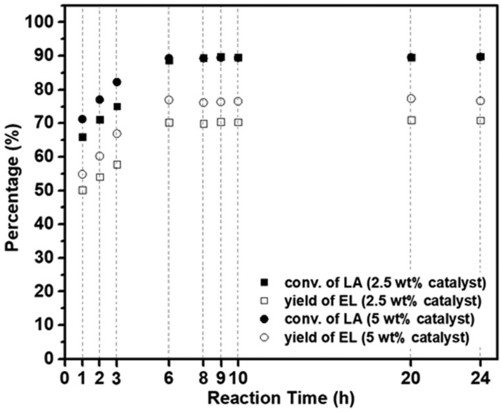

Fig. 10 Catalytic performance of MM/Chi/GTMAC for esterification of LA with EtOH to EL. Reaction conditions: the temperature of 80 °C and EtOH/LA = 17.

Here, we compared the catalytic performance of our catalyst with previously reported ones which are summarized in Table 3 with the given reaction condition. Unfortunately, since few base-catalyzed esterifications of LA have been reported, we compared our results with those obtained using acid catalysts. Compared to the catalytic performances in previous reports, our catalyst (MM/Chi/GTMAC) shows comparable performance, so it can be concluded that our result is at least as good as theirs. In addition, we want to emphasize that quaternary ammonium salt (GTMAC) is environmentally friendly and prevents the environment from contamination.[22] Introducing a magnetic property in the base catalyst offers another benefit: the catalyst is easily separated from the system with an external magnet after the reaction.

Identification of by-products formed by the reaction. Since LA has two functional groups, ketone and carboxyl groups, two reactions involving each functional group are possible, where one is the formation of EL (desired product) and the other giving an undesired by-product by cyclization of LA (Fig. 11).

Table 3 Levulinic acid esterification over various catalysts in previous reports

Catalyst	Condition	Conv. (%)	Yield (%)
Porous sulfonated carbon[47]	LA : EtOH (1 : 5); 8 h; 80°	94	NA
Carbon cryogel[28]	LA : EtOH (1 : 12); 3 h; 78 °C	90	86.5
Amberlite IR120[48]	LA : EtOH (1 : 15); 4 h; 150 °C	86.5	85
1-Ethyl-3-mehylimidazolium tosylate ([EMim][OTS])[49]	LA : EtOH (1 : 10); 5.25 h; 90 °C	84	78
ZSM-12 nanolayers[50]	LA : EtOH (1 : 1); 24 h; 100 °C	78.5	NA
SO_4^{2-}/SnO_2[51]	LA : EtOH (1 : 15); 7 h; 70 °C	77	NA
SiO_2–SO_3H[11]	LA : EtOH (1 : 10); 4 h; 70 °C	70.6	NA
MM/Chi/GTMAC (this work)	LA : EtOH (1 : 17); 6 h; 80 °C	89	77

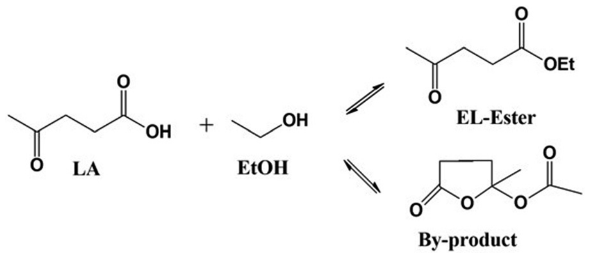

Fig. 11 Formations of EL and the by-product in the esterification of LA with EtOH.

Table 4 Kinetic analyses for the reaction over MM/Chi/GTMAC

Reaction order	Linear regression	R^2 value
Pseudo-zeroth	$y = 0.0478x + 0.6737$	0.9623
Pseudo-first	$y = 0.0557x - 2.7784$	0.9833
Pseudo-second	$y = 1.6342x + 1.4374$	0.9504

GC-FID analysis of the reaction solution at a certain reaction time suggested the formation of by-products because the yield of EL was lower than the conversion of LA. To confirm the formation of by-products, GC–MS analysis was performed, and the results are presented in Fig. S2 in ESI.† The existence of a by-product was clearly shown on the chromatograms (Fig. S2a and b, ESI†). To identify the by-product, we took MS spectrum of the by-product, and it was revealed that the by-product was 2-methyl-5-oxotetrahydro-2-furanyl acetate (Fig. S2c in ESI†). Because this compound is an intermediate in the esterification reaction of LA with EtOH, which is called pseudo-ester, it is challenging to suppress the formation of this compound completely.

Kinetics. Kinetic analysis for the esterification of LA with EtOH catalyzed by MM/Chi/GTMAC was studied at 80 °C. By applying eqn (6)–(8) to the reaction data, how the reaction proceeded, namely, which of pseudo-zeroth-order, pseudo-first-order, and pseudo-second-order kinetics was more plausible,

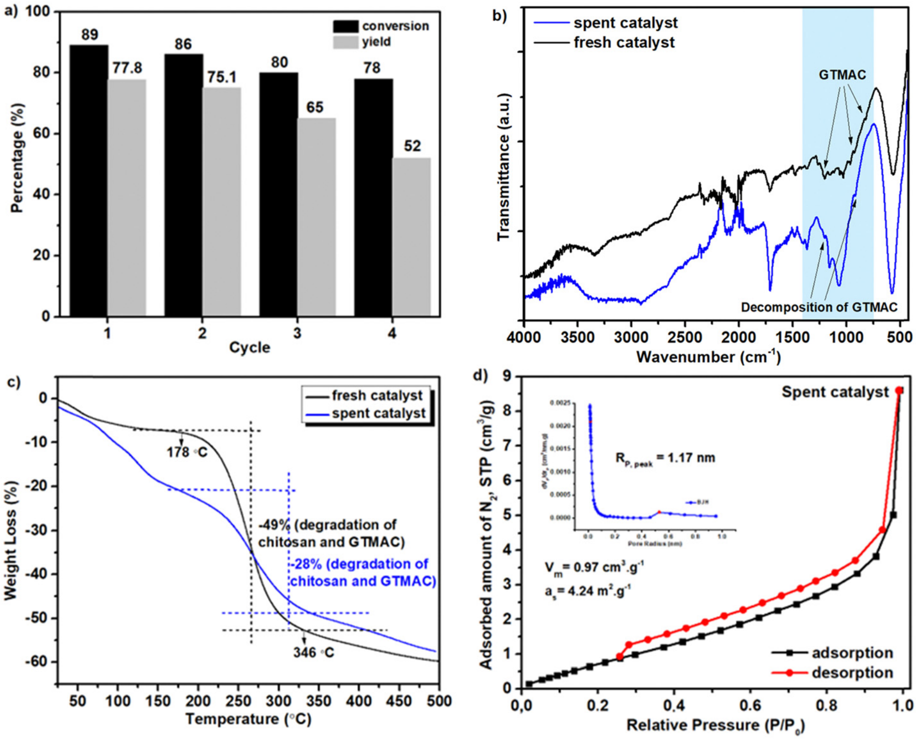

Fig. 12 (a) Result of the catalyst reusability test, (b) IR spectra, (c) TGA curve, (d) pore and surface characterization of the spent catalyst.

was investigated. The linear plots of these reaction kinetic models are shown in Fig. S3 (ESI†), and Table 4 summarizes the correlation coefficients (R^2) for the three kinetic models. The R^2 value of the pseudo-first-order model was the closest to 1. Judging from the R^2 value, therefore, the pseudo-first-order model was the most plausible, and the reaction rate constant, $k'_{1,1}$, was estimated to be 2.42×10^{-2} min^{-1}. This value is comparable to the esterification of LA with EtOH over previously reported solid acid catalyst, which is SiO_2–SO_3H modified with methyl group (5.40×10^{-3} min^{-1}).[11]

Catalyst reusability. The reusability of a catalyst is a vital indicator that must be considered as one of the catalytic performances. The reusability of MM/Chi/GTMAC was evaluated by conducting the reaction repeatedly under the optimum reaction conditions (80 °C and 6 h). As shown in Fig. 12(a), each repeated use decreased the catalytic performance gradually. The reaction using the fresh catalyst achieved 89% conversion and 77% yield, and those after four cycles were 78% conversion and 52% yield. A possible reason for the decrease in the catalytic performance was the elution of the active components into the reaction solution or washing-up liquid. This speculation was supported by the characterization of the spent catalyst, which clearly showed a decrease in the amount of GTMAC in the spent catalyst (Fig. 12(b) and (c)) and a decrease in the porosity (Fig. 12(d)). As the IR spectrum of the spent catalyst shows (Fig. 12(b)), the characteristic peaks due to GTMAC were significantly weakened. In addition, the decrease in the organic component content, including chitosan and GTMAC, was also confirmed on the TG profile of the spent catalyst (Fig. 12(c)). Improvement of the durability of the catalyst is one of the challenges for the future, and we continue to work on it.

4. Conclusions

In this study, a novel composite material (MM/Chi/GTMAC) has been successfully synthesized by modifying MM with chitosan and GTMAC in sequence. The structure and properties of MM/Chi/GTMAC were comprehensively characterized with various physical and chemical methods, and it was found that base sites were successfully introduced to the composite material by modification with GTMAC. This composite material acted as a heterogeneous base catalyst and effectively promoted the esterification of LA with EtOH to produce EL due to the basicity of chloride ions. This heterogeneous base catalyst was magnetically separable and reusable for the esterification, though the catalytic performance decreased gradually with each repeated use.

Author contributions

The manuscript was written through the contributions of all authors. All authors have approved the final version of the manuscript. Feri Mukhayani: methodology, investigation, data visualization, writing – original draft; Nuryono, Yuichi Kamiya, Ryoichi Otomo, and Eko Sri Kunarti: conceptualization, resources, formal analysis, writing – review and editing.

Conflicts of interest

There are no conflicts to declare.

Acknowledgements

All authors thank Indonesia's Ministry of Education, Culture, Research, and Technology for the financial support through the Enhancing International Program (EIP-PMDSU) within contract no. 2192/UN1/DITLIT/Dit-Lit/PT.01.03/2023, the Scientific Publication Quality Improvement Program with contract no. 165.23/E4.4/KU/2023, and Promotor Collaboration Improvement Program with contract no. 224/E4.4/KU/2023. A part of this work was conducted at the Laboratory of XPS and SQUID-VSM analysis, Joint-use facilities, Hokkaido University.

References

1 S. Heger, K. Bluhm, J. Brendt, P. Mayer, N. Anders, A. Schaffer, T. B. Seiler and H. Hollert, Microscale in Vitro Assays for the Investigation of Neutral Red Retention and Ethoxyresorufin-*O*-Deethylase of Biofuels and Fossil Fuels, *PLoS One*, 2016, **11**, 1–24.
2 S. K. Hoekman, A. Broch, C. Robbins, E. Ceniceros and M. Natarajan, Review of biodiesel composition, properties, and specifications, *Renewable Sustainable Energy Rev.*, 2012, **16**, 143–169.
3 B. C. Windom, T. M. Lovestead, M. Mascal, E. B. Nikitin and T. J. Bruno, Advanced Distillation Curve Analysis on Ethyl Levulinate as A Diesel Fuel Oxygenate and A Hybrid Biodiesel Fuel, *Energy Fuels*, 2011, **25**, 1878–1890.
4 C. C. L. McCrory, S. Jung, I. M. Ferrer, S. M. Chatman and J. C. Peters, T. F. Jaramillo, Benchmarking Hydrogen Evolving Reaction and Oxygen Evolving Reaction Electrocatalysts for Solar Water Splitting Devices, *J. Am. Chem. Soc.*, 2015, **137**, 4347–4357.
5 W. Ying, Z. Longbao and W. Hewu, Diesel Emission Improvements by the Use of Oxygenated DME/Diesel Blend Fuels, *Atmos. Environ.*, 2006, **40**, 2313–2320.
6 L. M. Schmidt, L. D. Mthembu, P. Reddy, N. Deenadayalu, M. Kaltschmitt and I. Smirnova, Levulinic Acid Production Integrated into A Sugarcane Bagasse Based Biorefinery Using Thermal-Enzymatic Pretreatment, *Ind. Crops Prod.*, 2017, **99**, 172–178.
7 B. Girisuta and H. J. Heeres, Levulinic Acid from Biomass: Synthesis and Applications, in *Production of Platform Chemicals from Sustainable Resources*, ed. Z. Fang, R. L. Smith and X. Qi, Biofuel and Biorefineries, Springer, Singapore, 2017, pp. 143–169, DOI: 10.1007/978-981-10-4172-3_5.
8 G. D. Yadav and A. R. Yadav, Synthesis of Ethyl Levulinate as Fuel Additives Using Heterogeneous Solid Superacidic Catalysts: Efficacy and Kinetic Modeling, *Chem. Eng. J.*, 2014, **243**, 556–563.
9 F. Link, N. Ahad and A. De Klerk, Low-Pressure Hydrocracking of Wax over Pt/SiO_2–Al_2O_3 to Produce Kerosene for Synthetic Jet Fuel, *ACS Symp. Ser.*, 2021, **1379**, 311–352.

10 A. H. Hassan, M. M. Zainol, M. A. Samion, M. A. Azlan, M. Asmadi, A. R. Mohamad Daud, I. Saad and N. A. N. M. Nor Azman, Synthesis of Ethyl Levulinate Over Sulfonated Lignin-Based Carbon Catalyst as A Fuel Additive to Biodiesel-Diesel Blends Towards Engine Emissions, *J. Cleaner Prod.*, 2023, **418**, 138101.

11 D. D. Ristiana, S. Suyanta and N. Nuryono, Sulfonic Acid-Functionalized Silica with Controlled Hydrophobicity as an Effective Catalyst for Esterification of Levulinic Acid, *Mater. Today Commun.*, 2022, **32**, 103953.

12 D. D. Ristiana, S. Suyanta and N. Nuryono, Simple One-Pot Synthesis of Sulfonic-Acid-Functionalized Silica for Effective Catalytic Esterification of Levulinic Acid, *Indones. J. Chem.*, 2021, **22**, 157–170.

13 D. T. Melfi, M. K. Lenzi, L. P. Ramos and M. L. Corazza, Kinetic Modeling of $ScCO_2$-Assisted Levulinic Acid Esterification with Ethanol Using Amberlyst-15 as a Catalyst in a Batch Reactor, *Energy Fuels*, 2021, **35**, 14770–14779.

14 A. H. Hassan, M. M. Zainol, K. R. Zainuddin, H. A. Rosmadi, M. Asmadi, N. A. Rahman and N. A. S. Amin, A Review on Alkyl Levulinates Synthesis from Renewable Levulinic Acid using Various Modified Carbon-Based Catalysts, *Malays. J. Chem.*, 2022, **24**, 264–282.

15 D. W. Lee, Y. M. Park and K. Y. Lee, Heterogeneous Base Catalysts for Transesterification in Biodiesel Synthesis, *Catal. Surv. from Asia*, 2009, **13**, 63–77.

16 M. Jayakumar, N. Karmegam, M. P. Gundupalli, K. Bizuneh Gebeyehu, B. Tessema Asfaw, S. W. Chang, B. Ravindran and M. K. Awasthi, Heterogeneous Base Catalysts: Synthesis and Application for Biodiesel Production – A Review, *Bioresour. Technol.*, 2021, **331**, 125054.

17 A. G. Margellou, A. A. Koutsouki, D. E. Petrakis, M. G. Kontominas and P. J. Pomonis, Catalysis and Inhibition of Transesterification of Rapeseed Oil over MgO–CaO, *BioEnergy Res.*, 2023, **16**, 528–538.

18 A. Mukhtar, S. Saqib, H. Lin, M. U. Hassan Shah, S. Ullah, M. Younas, M. Rezakazemi, M. Ibrahim, A. Mahmood, S. Asif and A. Bokhari, Current Status and Challenges in the Heterogeneous Catalysis for Biodiesel Production, *Renewable Sustainable Energy Rev.*, 2022, **157**, 112012.

19 C. Li, S. Zhao, X. Yao, L. He, S. Xu, X. Shen and Z. Yao, The Catalytic Mechanism of Intercalated Chlorine Anions as Active Basic Sites in Mgal-Layered Double Hydroxide for Carbonyl Sulfide Hydrolysis, *Environ. Sci. Pollut. Res.*, 2022, **29**, 10605–10616.

20 F. Cheng, J. Yang, L. Yan, J. Zhao, H. Zhao, H. Song and L. Chou, Impact of Chloride Ions on the Oxidative Coupling of Methane Over Li/Sno_2 Catalyst, *React. Kinet., Mech. Catal.*, 2018, **125**, 675–688.

21 R. B. Istiningrum, S. J. Santosa and N. Nuryono, Preparation of Magnetic/silica/quarternary-chitosan by Sol-Gel Method and Its Stability in Various pH Medium, *Rasayan J. Chem.*, 2021, **14**, 2767–2775.

22 S. P. Rwei, Y. M. Chen, W. Lin and W. Y. Chiang, Synthesis and Rheological Characterization of Water-Soluble Glycidyltrimethylammonium-Chitosan, *Mar. Drugs*, 2014, 5547–5562.

23 A. M. Sajjan, B. K. Jeevan Kumar, A. A. Kittur and M. Y. Kariduraganavar, Development of Novel Grafted Hybrid PVA Membranes Using Glycidyltrimethylammonium Chloride For Pervaporation Separation of Water–Isopropanol Mixtures, *J. Ind. Eng. Chem.*, 2013, **19**, 427–437.

24 K. Wang, F. Zhang, K. Xu, Y. Che, M. Qi and C. Song, Modified Magnetic Chitosan Materials for Heavy Metal Adsorption: A Review, *RSC Adv.*, 2023, **13**, 6713–6736.

25 T. M. Budnyak, I. V. Pylypchuk, V. A. Tertykh, E. S. Yanovska and D. Kolodynska, Synthesis and Adsorption Properties of Chitosan-Silica Nanocomposite Prepared by Sol-Gel Method, *Nanoscale Res. Lett.*, 2015, **10**, 87.

26 N. Nuryono, D. Miswanda, S. C. W. Sakti, B. Rusdiarso, P. A. Krisbiantoro, N. Utami, R. Otomo and Y. Kamiya, Chitosan-Functionalized Natural Magnetic Particle@Silica Modified with (3-Chloropropyl)Trimethoxysilane as A Highly Stable Magnetic Adsorbent for Gold(III) Ion, *Mater. Chem. Phys.*, 2020, **255**, 123507.

27 F. W. Mahatmanti and N. Nuryono, Physical Characteristics of Chitosan Based Film Modified with Silica and Polyethylene Glycol, *Indones. J. Chem.*, 2014, 131–137.

28 M. M. Zainol, N. A. S. Amin and M. Asmadi, Kinetics and Thermodynamic Analysis of Levulinic Acid Esterification Using Lignin-Furfural Carbon Cryogel Catalyst, Renew, *Energy*, 2019, **130**, 547–557.

29 T. A. Degfie, T. T. Mamo and Y. S. Mekonnen, Optimized Biodiesel Production from Waste Cooking Oil (WCO) using Calcium Oxide (CaO) Nano-catalyst, *Sci. Rep.*, 2019, **9**, 18982.

30 S. Lotfi, F. Ghaderi, A. Bahari and S. Mahjoub, Preparation and Characterization of Magnetite–Chitosan Nanoparticles and Evaluation of Their Cytotoxicity Effects on MCF7 and Fibroblast Cells, *J. Supercond. Novel Magn.*, 2017, **30**, 3431–3438.

31 F. Shi, Y. Li, Q. Zhang and H. Wang, Synthesis of Fe_3O_4/C/TiO_2 Magnetic Photocatalyst via Vapor Phase Hydrolysis, *Int. J. Photoenergy*, 2012, 365401.

32 N. E. A. El-Naggar, A. M. Shiha, H. Mahrous and A. B. A. Mohammed, Green Synthesis of Chitosan Nanoparticles, Optimization, Characterization and Antibacterial Efficacy Against Multi-Drug Resistant Biofilm-Forming *Acinetobacter Baumannii*, *Sci. Rep.*, 2022, **12**, 1–19.

33 M. F. Queiroz, K. R. T. Melo, D. A. Sabry, G. L. Sassaki and H. A. O. Rocha, Does the Use of Chitosan Contribute to Oxalate Kidney Stone Formation?, *Mar. Drugs*, 2015, **13**, 141–158.

34 Z. Sekhavat Pour, P. Makvandi and M. Ghaemy, Performance Properties and Antibacterial Activity of Crosslinked Films of Quaternary Ammonium Modified Starch and Poly(Vinyl Alcohol), *Int. J. Biol. Macromol.*, 2015, **80**, 596–604.

35 L. Y. Huang, W. Li, N. Du, H. Q. Lu, L. D. Meng, K. Y. Huang and K. Li, Preparation of Quaternary Ammonium Magnetic Chitosan Microspheres and Their Application for Congo Red Adsorption, *Carbohydr. Polym.*, 2022, **297**, 119995.

36 T. A. Dickstein, E. Zhou, K. K. Hershberger, A. K. Haskell, D. G. Morgan, M. Pink, B. D. Stein, L. Z. Nikoshvili,

V. G. Matveeva and L. M. Bronstein, Chitosan as Capping Agent in A Robust One-Pot Procedure for A Magnetic Catalyst Synthesis, *Carbohydr. Polym.*, 2021, **269**, 118267.

37 D. Wilson and M. A. Langell, MA, XPS Analysis of Oleylamine/Oleic Acid Capped Fe_3O_4 Nanoparticles as a Function of Temperature, *Appl. Surf. Sci.*, 2014, **303**, 6–13.

38 S. Favela-Camacho, E. Samaniego, A. Godínez-García, L. Aviles-Arellano and J. F. Pérez-Robles, How to Decrease the Agglomeration of Magnetite Nanoparticles and Increase Their Stability Using Surface Properties, *Colloids Surf., A*, 2019, **1**, 574.

39 F. P. Ramanery, A. A. P. Mansur and H. S. Mansur, One-step Colloidal Synthesis of Biocompatible Water-Soluble ZnS Quantum Dot/Chitosan Nanoconjugates, *Nanoscale Res. Lett.*, 2013, **8**, 1–13.

40 A. Chenite, M. Buschmann, D. Wang, C. Chaput and N. Kandani, Rheological Characterisation of Thermogelling Chitosan/Glycerol-Phosphate Solutions, *Carbohydr. Polym.*, 2000, **46**, 39–47.

41 T. Puangkaew, N. Booranabunyat, S. Kiatkamjornwong, P. Thanyasrisuung and V. P. Hoven, Amphiphilic Quaternized Chitosan: Synthesis, Characterization, and Anti-Cariogenic Biofilm Property, *Carbohydr. Polym.*, 2022, **277**, 118882.

42 I. Aranaz, A. R. Alcántara, M. C. Civera, C. Arias, B. Elorza, A. Heras Caballero and N. Acosta, Chitosan: An Overview of Its Properties and Applications, *Polymers*, 2021, **13**, 3256.

43 V. M. Lenart, R. de Fátima Turchiello, M. P. Calatayud, G. F. Goy and S. L. Gómez, Synthesis of Magnetite Nanoparticles of Different Size and Shape by Interplay of Two Different Surfactants, *Braz. J. Phys.*, 2019, **49**, 829–835.

44 D. Zhang, L. Shang, J. Shen, Z. Shi, L. Wu, C. Tung and T. Zhang, A Mild One-Step Solvothermal Route to Truncated Octahedral Magnetite Crystals, *Particuology*, 2014, **15**, 51–55.

45 J. Guo, Z. Zheng, C. Chen, X. Lu, Y. Zhang and B. Zheng, Enhanced Production of κ-Carrageenase and κ-Carrageenan Oligosaccharides through Immobilization of *Thalassospira sp.* Fjfst-332 with Magnetic Fe_3O_4-Chitosan Microspheres, *J. Agric. Food Chem.*, 2017, **65**, 7934–7943.

46 J. Stejskal, I. Sapurina, J. Vilčáková, M. Jurča, M. Trchová, Z. Kolská, J. Prokes and I. Krivka, One-Pot Preparation of Conducting Melamine/Polypyrrole/Magnetite Ferrosponge, *ACS Appl. Polym. Mater.*, 2021, **3**, 1107–1115.

47 N. Li, Q. Wang, S. Ullah, X. C. Zheng, Z. K. Peng and G. P. Zheng, Esterification of Levulinic Acid in the Production of Fuel Additives Catalyzed by Porous Sulfonated Carbon Derived from Pine Needle, *Catal. Commun.*, 2019, **129**, 105755.

48 V. Russo, R. Tesser, C. Rossano, T. Cogliano, R. Vitiello, S. Leveneur and M. Di Serio, Kinetic Study of Amberlite IR120 Catalyzed Acid Esterification of Levulinic Acid with Ethanol: from Batch to Continuous Operation, *Chem. Eng. J.*, 2020, **401**, 126126.

49 L. D. Mthembu, D. Lokhat and N. Deenadayalu, Esterification of levulinic Acid to Ethyl Levulinate: Optimization of Process Conditions Using Commercial Levulinic Acid and Extension to The Use of Levulinic Acid Derived from Depithed Sugarcane Bagasse, *Biomass Convers. Biorefin.*, 2023, **13**, 3113–3122.

50 P. Dugkhuntod, T. Imyen, W. Wannapakdee, T. Yutthalekha, S. Salakhum and C. Wattanakit, Synthesis of Hierarchical ZSM-12 Nanolayers for Levulinic Acid Esterification with Ethanol to Ethyl Levulinate, *RSC Adv.*, 2019, **9**, 18087–18097.

51 M. Popova, P. Shestakova, H. Lazarova, M. Dimitrov, D. Kovacheva, A. Szegedi, G. Mali, V. Dasireddy and B. Likozar, Efficient Solid Acid Catalysts Based on Sulfated Tin Oxides for Liquid Phase Esterification of Levulinic Acid with Ethanol, *Appl. Catal., A*, 2018, **560**, 119–131.